IOP Publishing Journal of Physics A: Mathematical and Theoretical
J. Phys. A: Math. Theor. **47** (2014) 285201 (20pp) doi:10.1088/1751-8113/47/28/285201

High resolution portrait of the ideal trefoil knot

Sylwester Przybyl and Piotr Pieranski

Laboratory of Computational Physics, Poznan University of Technology, Nieszawska 5B/11, 60-965 Poznan, Poland

E-mail: Sylwester.Przybyl@put.poznan.pl

Received 25 February 2014, revised 22 April 2014
Accepted for publication 8 May 2014
Published 25 June 2014

Abstract

The shape of the tightest polygonal trefoil knot with $N = 200\,640$ vertices, constructed by the authors using an appropriately modified finite element method, is carefully analyzed. The large number of vertices provide a spatial structure with very precise plots of its curvature and torsion. Based on the increased accuracy of the data, the authors are able to formulate new conjectures concerning the key features of the shape of the ideal trefoil knot.

Keywords: knot, curvature, torsion, trefoil knot, ideal knot
PACS numbers: 36.20.2r, 46.70.2p, 87.19.2j

S Online supplementary data available from stacks.iop.org/JPhysA/47/285201/mmedia

(Some figures may appear in colour only in the online journal)

1. Introduction

Knots tied in a rope change their shape when tightened by making the rope shorter. Conformations at which the length/diameter ratio reaches its global minimum are often referred to as *ideal*. As proven by Cantarella *et al*, see theorem 7 in [1], such conformations, called minimizers, exist for all (tame) knots and links. They are $C^{1,1}$ with a bounded curvature. Although many works have been devoted to the problem, the ideal conformations of knots, even as simple as the trefoil knot, are only vaguely known today. It is the aim of the present paper to describe the results of a numerical simulation that allowed us to generate a portrait of the ideal trefoil knot at such a high resolution that new, essential details of its shape become clearly visible. Some of the details look unusual at the first sight. One may suspect that they are just products of the discrete nature of the simulated knot. To exclude this possibility we performed, with similar precision, numerical simulations of the simple clasp—a system

whose geometrical details have been discovered analytically. As we shall demonstrate, our simulation method is able to reproduce the details. Thus, the similar subtle details that we see in the structure of the tight trefoil knot are by all means a reality and not products of our simulation method.

2. The continuous trefoil knot and problems with numerical simulations of its tightening

The tightening of the closed knots requires a hypothetical process, in which the length of the rope diminishes while the diameter of its perpendicular sections remains constant. Let us note that for a closed knot its length is defined simply as the length of the rope in which the knot is tied. The longitudinally shrinking rope comes into contact with itself. When the surface of the rope is slippery, and when the rope is hard, the self-contact points move along its surface without any hindrance. As a result, the knot changes its shape until a conformation is reached at which the tightening process stops. Once again, the computer experiments indicate that for larger closed knots one may expect many tight conformations, which one arrives at from different initial conformations [2].

The physical properties of the perfect rope induce particular geometrical properties in the knots that are tied in it. The assumption that the rope is hard, i.e. its circular sections are not deformable and cannot overlap, implies that its axis has a continuous, but not necessarily smooth, tangent vector. As a result, its curvature versus the arclength function $\kappa(l)$, must remain free from any Dirac-delta-like components, but does not need to be continuous. Obviously, as explained above, it cannot be larger than $1/R$.

The tightening process performed on the trefoil knot tied in the perfect rope has been simulated in the past using different numerical procedures. The procedure, SP-FEM, used to obtain results described in the present paper, was an appropriately modified finite element method. Its detailed description will be published elsewhere. Unfortunately, such simulations are always awkward, since the unavoidable discretization of the knot results in dealing not with the knot itself, but with its discrete, polygonal representation. Let N be the number of vertices in the polygonal representation K_p of the simulated knot K. At the final analysis of the tightest conformation obtained from the numerical simulation, the tight polygonal knot K_p is replaced by a C^1 smooth knot K_c built from circular arcs inscribed into edges of the polygon. It seems natural to expect that as N becomes larger, the knot inscribed into the most tight polygonal knot better approximates the ideal conformation $\mathcal{K}_{\mathrm{id}}$. The toll paid for the discretization is high: at its full resolution, the curvature of the knot inscribed into the numerically found polygonal knot displays some features which are certainly not present in the ideal conformation and must be seen as artifacts of the discretization. To remove them and see the true shape of the knot, the resolution must be brought down. As a result, the image of the knot becomes more vague, but this allows us to see the true shape of the ideal conformation. When N is very large (of order 10^5), lowering the resolution ten times gives an image which is still precise enough to reveal subtle details of the knot shape.

3. Numerical simulation of the simple clasp

As forementioned, whilst performing numerical experiments we are constrained to work only with finite resolution portraits of the ideal conformation. By analyzing the portraits we are trying to guess what the shape of the ideal conformation is. A much better choice would be finding the ideal conformation via a rigorous analytical calculation. Unfortunately, nobody

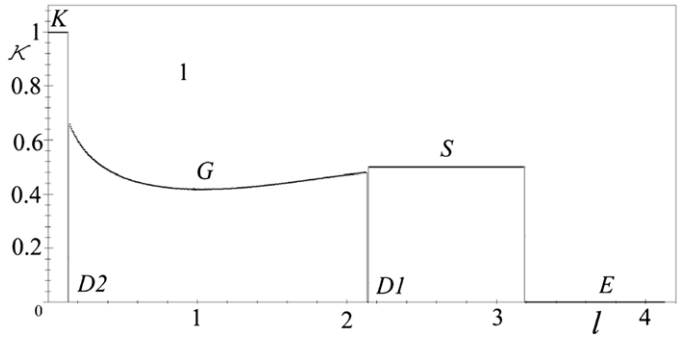

Figure 2. Curvature of the most tight simple clasp found by the SP-FEM simulation method. The plot stays in a quantitative agreement with the plot presented by Starostin [4].

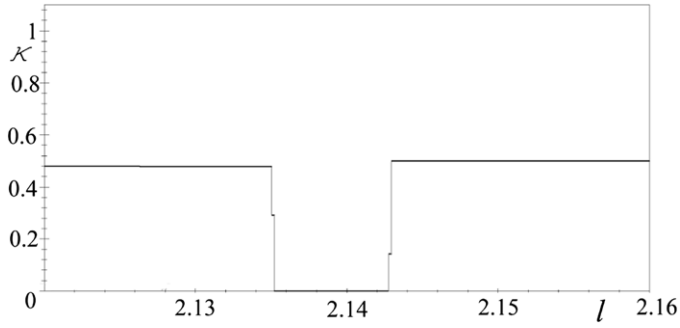

Figure 3. Curvature in the *D1* region of the simple clasp. The length of the straight piece equals 0.008, which stays in a quantitative agreement with Starostin's solution [4].

curvature of the clasped ropes. Within the Gehring piece the rope stays in a double touch with the other rope along two curved lines. Curvature changes here in a smooth manner. The last curved piece of the simple clasp structure is located at the center. SSC call it *kink* (*K*). Within the kink piece, the rope stays in touch with itself. This happens at a single point, where the circular sections of the rope are at a tangent to each other. Curvature here reaches its highest allowable value $\kappa = 1$. Parts *E*, *S*, *G* and *K* are of comparable size and are easy to find in a numerical simulation. The problem is that, as SSC revealed, both between *S* and *G*, as well as between *G* and *K*, there are two additional, extremely short pieces *D*1 and *D*2, where the rope becomes straight, i.e. where curvature drops to zero. The length of the pieces is so small that in figures where SSC presented their solutions, they could not be visualized properly. Pieces *D*1 and *D*2 of the SSC solution are extremely short, but it does not mean we can neglect them. On the contrary, they should be seen as the fingerprints of the ideal conformation of the simple clasp. If they are not seen in a numerical simulation of the clasp, then either the simulated clasp is not tight, or the simulation is not precise enough. The SP-FEM simulation was subject to this precision test. In the simulation each of the clasp ropes was represented by a polygonal curve containing $N = 64\,001$ vertices. The plot of the curvature of half of one of the ropes is presented in figure 2. As one can see, all the pieces predicted by the SSC solution are there, although the *D*2 piece is not properly developed. (Our figure 2 can be confronted with figure 20 in [4].) The details of the curvature plot in the region of the *D*1 piece are presented in figure 3. As seen in the figure, the width of the *D*1 piece equals about 0.008. This is in agreement with the result of Starostin's calculation, who predicted 0.0078 [4]. Starostin's

calculation predicts the width of the $D2$ piece to be equal 0.0004, while the edge length of the polygonal curve representing the rope in our simulation was equal 0.000 13. This explains why the $D2$ piece seen in figure 2 is fully developed, i.e. curvature drops to zero. With the knowledge of how narrow the $D1$ and $D2$ pieces are, one immediately sees that finding them in a numerical simulation is not a trivial task. The SP-FEM method managed to complete this the task which gave us more confidence both in its in organization and precision.

Having reproduced the subtle details of the SSC solution, we have also understood that some unexpected, extremely narrow details, which we have previously seen in the simulated tight knots, may be not artifacts of the discretization, but essential parts of the ideal conformations. The case of the tight overhand knot considered in [7] needs to be re-analyzed from this point of view using a higher precision simulation.

4. The pursuit for the ideal trefoil knot: a retrospection

Looking into the history of the ideal trefoil knot problem we see how, step by step, using various numerical knot tightening procedures such as simulated inflation (SI) [8], shrink-on-no-overlaps (SONO) [9], deterministic ropelength minimizing algorithm (DRMA) [10], simulated annealing [11] and constrained gradient descent (ridgerunner) [12], conformations of shorter and shorter ropelength have slowly been found. (The *ropelength* of a knot is the ratio of the length of the rope, in which the knot is tied, to the radius of the rope. In terms of the notation used in the present paper, putting $R = 1$ turns the length L into ropelength.) Since, as a rule, at larger N shorter conformations were found together with shorter knots, new details of the anatomy for the ideal trefoil knot were discovered and new conjectures concerning its shape were formulated. It is the aim of the present paper to describe a few new details revealed in the simulations carried out with the use of the appropriately adapted finite element method (SP-FEM). The details are essential as they change our view on the shape of the ideal trefoil conformation. Before we present them, let us briefly summarize what is currently known about the ropelength of the ideal trefoil knot.

The hypothetical process described above, in which the knot becomes tightened because the rope in which it has been tied shrinks longitudinally while keeping its diameter intact or keeping its length intact increases its diameter, was realized for the first time in practice within the virtual reality computer simulations by Katritch *et al* [8]. The minimum length of the trefoil knot determined in the simulations was equal to 32.8, although the method with which the number had been determined was not described in the paper. The first precisely defined value of the ropelength of the tight trefoil was given by Rawdon [10] who developed a clear method with which the value should be calculated. The value given by Rawdon was equal to 32.80. An extensive study of the dependence of the ropelength L of trefoil knots on the number of vertices N used for their discretization was described by Baranska *et al* [13]. The aim of the study was to estimate the ropelength of the tight polygonal trefoil knots found by the SONO algorithm in the $N \to \infty$ limit. To achieve this goal, trefoil knots with $N = 1008, 1128, 1272, 1416, 1584, 1776, 2016, 2256$ and 2544 vertices were tightened with the use of the SONO algorithm. Analyzing the dependence $L(N)$ the authors arrived at the conclusion that as $N \to \infty$ the ropelength should asymptotically approach the value 32.742 95. (The results of the study presented in the next section will allow us to comment this prediction). Let us emphasize that the above value is an approximate prediction. As far as the exact numerically provable values of the ropelength upper bounds are concerned, the length of the shortest trefoil knot was equal to 32.7434. It was found for a knot with $N = 2544$ vertices [13]. A slightly shorter knot with $N = 3552$ vertices was found with the use of the SONO

Table 1. Ropelength values obtained by various authors. SI—simulated inflation, SONO—shrink-on-no-overlaps, DRMA—deterministic ropelength minimizing algorithm, SA—simulated annealing, CGD—constrained gradient descent, SP-FEM—finite element method. The knots analyzed in papers [13, 14] were found by the Przybyl method. Ropelength values marked with a question mark were calculated with a method that was not clearly specified.

Author	Method	N	L
Katritch *et al* 1996 [8]	SI	160	32.8
Pieranski *et al* 2001 [15]	SONO	327	32.76
Rawdon 2003 [10]	DRMA	160	32.90
Baranska *et al* 2004 [13]	SONO	2544	32.7434
Carlen *et al* 2006 [11]	SA	528 (arcs)	32.7444
Baranska *et al* 2008 [14]	SONO	3552	32.7432
Ashton *et al* 2011 [12]	CGD	2400	32.7437
Przybyl *et al* (present paper)	SP-FEM	200 640	32.742 9345

algorithm a few years later [14]. Its ropelength was equal to 32.7432. The shortest trefoils found by the RIDGERUNNER algorithm [12] and by the simulated annealing technique [11] are a bit longer: 32.7437 and 32.7444, respectively. The knot that we are presenting below contains $N = 200\,640$ vertices and is shorter than any of the previously found knots. Its ropelength equals 32.742 9345, i.e. even less than the previously predicted 32.742 95 value [13]. The results from the pursuit for the determination of the ideal trefoil knot ropelength are gathered in table 1.

It may seem that the differences between the consecutive ropelength results presented above are so small that one should not bother about them. This is not the case. Although small, the differences are by no means negligible. On the contrary, they are essential; by finding a conformation with a slightly lower value of the ropelength we are getting closer to the ideal conformation and its portrait has a superior resolution. The essential details of the ideal trefoil only anatomy become visible when the resolution is high enough.

The ropelength is just a single parameter in characterizing the tight knot found by numerical simulation and it is of course desirable to know it: the lower the ropelength value, the closer the found knot to the ideal one. However, as a single geometrical parameter the ropelength does not tell us anything about the shape of the knot. To gain insight into the shape, we must look at the plots of the curvature and torsion versus the arclength parameter: $\kappa(l)$ and $\tau(l)$. The plots should be very precise indeed, since they may contain the small, but essential, details we have demonstrated considering the simple clasp structure above.

The curvature and torsion functions give an exact and complete description of their shape. (To make the description unambiguous, we must allow the torsion function to contain the Dirac-delta-like components.) By observing the plots of curvature and torsion one is able to indicate regions of the knot in which the rope has some well defined shapes, e.g. arcs or helices. The problem we face is that the torsion plots of tighter conformations, found by various knot tightening programs, display a high level of noise, because the numerical calculation of torsion needs the third derivative of the position vector field.

One of the first papers in which essential conjectures of the ideal trefoil knot shape were formulated was published by Carlen *et al* [11]. Knots analyzed by the Lausanne team were approximated by bi-arcs. The tightest trefoil knot they managed to find after '*...several months of simulated annealing computation*' was built from 265 bi-arcs, thus, from $N = 528$ arcs of varying length. The reported ropelength was $L = 32.744$. The authors study the knot in detail with the aim of formulating some conjectures concerning its shape. They calculate the radii of all the arcs obtaining a plot, see figure 3(*a*) [11], which reflects the curvature of the knot.

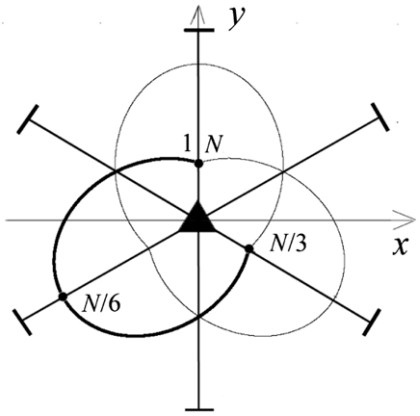

Figure 4. Vertex numbering and basic symmetry elements of the K_p knot. Existence of the three- and two-fold symmetry axes allows one to limit analysis of the knot to $1/6$ part of it.

The analysis of the plot, supported by analysis of the contact set, led the authors to state the following.

Conjecture 1 (Carlen *et al* [11])**.** *We remark that local radii are not active in the contact set for* $\mu^* = 8.1861 \times 10^{-6}$*, but are remarkably close to being active. For example local curvature does form part of the contact set* $\chi_{5\mu^*}$*. Thus it is quite possible that on the true ideal shape local curvature does achieve thickness at six distinct points.*

Looking at the figure one can see that indeed one of the bi-arc curvature radii seems to reach its lowest allowable value of the rope radius but at the five other minima the plot of the radii values remains clearly above the limit.

As far as the torsion is concerned, the authors of [11] did not plot its values, instead, they plotted unsigned values of the angles between planes of the oscillating circles of the successive arcs. See figure 4 [11]. Analysis of this plot led the authors to formulate the following conclusion.

Conjecture 2 (Carlen *et al* [11])**.** *There are three regions with large angles that correspond to the regions with a high variation of the radii, that is to the parts of the curve inside the knot. Note that the angle is given in radians, that is, the maximal value of around 1.2 between adjacent arcs corresponds to an angle of around 70 degrees. These extremely large values could lead to the speculation that the Frenet frame of the underlying ideal curve may be discontinuous, and that the associated ideal centerline curve may not be* C^2 *at nearby points.*

The conjectures formulated by Carlen *et al* [11] can be confronted with the results of analysis performed by Baranska *et al* [14]. The knot analyzed by the authors contained $N = 3550$ vertices. It was found after several hours of simulation was performed with the use of the SONO algorithm. The knot was highly equilateral: the relative deviation of the length of its edges from the average length was less than 10^{-7}. Its ropelength, calculated by the method developed by Rawdon [10], was $L = 32.743\,17$, thus the knot was tighter than the knot analyzed by Carlen *et al* As clearly seen in figure 15 in [14], where the curvature of the $N = 3552$ knot is in the region of one of the double peaks, the first conjecture formulated by Carlen *et al* is too weak. The curvature indeed achieves its upper limit value, but this happens not at six distinct points, but on six finite intervals. The speculation formulated by

Carlen *et al* concerning the torsion of the ideal knot is not found in the analysis performed by Baranska *et al*, neither a confirmation nor contradiction [14]. The torsion data proved also to be very noisy. This forced the authors to use a smoothing procedure. The smoothing allowed them to plot torsion and indicate in the plot three double maxima, but excluded the possibility of proving or disproving the speculations concerning the continuity or discontinuity of the orientation of the Frenet frame. Another effort to find a tight conformation of the trefoil knot was made by Ashton *et al* with the use of the constrained gradient descent method [12]. The tightest trefoil knot they managed to find contained $N = 2400$ vertices. Its ropelength L was equal to 32.743 663 which is more than the ropelength of the $N = 3552$ trefoil found by Przybyl [14]. The result that the curvature hits its upper limit on six intervals has been confirmed. This is clearly seen in figure 13 of [12], where curvature is plotted. The question of the torsion plot was not considered.

5. The ideal trefoil as seen in its $N = 200\,640$ vertices portrait

The extremely tight and precise polygonal trefoil knot K_p containing $N = 200\,640$ which we are going to present and analyze was found by one of us (SP) in a simulation performed with the use of the appropriately modified finite element method (SP-FEM). Numerical calculations simulating the tightening of the knot lasted (on a PC computer) a few months and were finished when the knot reached the state at which no further tightening was possible. A simple numerical analysis reveals that the K_p knot is highly symmetrical. Its symmetry is D_3. The knot has a single three-fold symmetry axis and three, perpendicular to it, two-fold axes. Thus, the knot consists of six congruent parts. In view of this, in analyzing the shape of the knot we shall limit the analysis to a representative 1/6 part of it. See figure 4. To make plots of curvature and torsion that will appear during this analysis compatible with the plots presented above for the simple clasp we have chosen, as the starting point of the arclength axis l, the point at which the central minimum within the double peaks of curvature is located. The vertex has an index equal to 1. See figure 4.

5.1. Length

Let the vertices of the polygonal knot K_p be denoted by $\boldsymbol{v}_i$. The average distance between consecutive vertices, i.e. the average length of its edges $\boldsymbol{e}_i$

$$e_{\mathrm{av}} = \frac{1}{N}\sum_{i=1}^{N} e_i = 1.631\,924\,564\,37 \times 10^{-4}, \tag{1}$$

where

$$e_i = \|\boldsymbol{e}_i\| = \|\boldsymbol{v}_{i+1} - \boldsymbol{v}_i\|. \tag{2}$$

Deviations of the segment lengths away from the average value are not larger than 2×10^{-15}. In view of this, the K_p knot can be treated as equilateral.

The length of the polygonal knot K_p is given with the accuracy stemming from the fluctuations of the length of its segments described above

$$L_p = \sum_{i=1}^{N} e_i = 32.742\,934\,460(1). \tag{3}$$

Following Rawdon [10], the polygonal knot K_p is replaced by the inscribed knot K_c. Since, as indicated above, the K_p knot can be considered as equilateral, the construction of the Rawdon inscribed knot becomes particularly simple: consecutive arcs a_i and a_{i+1} inscribed at

vertices $\boldsymbol{v}_i$ and $\boldsymbol{v}_{i+1}$ of the knot meet practically without any gap in the middle of the edge $\boldsymbol{e}_i = \boldsymbol{v}_{i+1} - \boldsymbol{v}_i$.

Let $\Delta l_i,\ i = 1, 2, \ldots, N$ be the lengths of the circular arcs, the union of which is K_c. The ropelength of the inscribed knot calculated with the Rawdon method gives:

$$L_c = \frac{\sum_{i=1}^{N} \Delta l_i}{R_c} = 32.742\,934\,547(1), \tag{4}$$

where

$$R_c = \sqrt{1 - \frac{e_{\mathrm{av}}^2}{4}} = 0.999\,999\,996\,67(1). \tag{5}$$

The L_c value given above can be seen as a new, numerically provable, upper bound for the ropelength of the ideal trefoil. The previously known bound, equal to 32.743 386, was given in [13].

Calculations presented in [13] show that the polygonal length underestimates the true ropelength of torus knots while the inscribed arcs length slightly overestimates it. The calculations indicate also that the true ropelength should be approximated well by an appropriately weighted average:

$$L_a = \tfrac{4}{5} L_p + \tfrac{1}{5} L_c. \tag{6}$$

Using this formula for the K_p and K_c knots we find:

$$L_a = 32.742\,934\,477(1). \tag{7}$$

The number can be seen as a new, more precise prediction of the ropelength of the ideal trefoil; the previous one, as predicted in [13] on the basis of knots tied with the SONO algorithm, was equal to 32.742 95.

5.2. Curvature and torsion

The ropelength of knot K_c, the shape of which we are going to analyze, is smaller than any from the previously found values. Thus, it is reasonable to assume that its structural details will be closer to those of the ideal trefoil knot $\mathcal{K}_{\mathrm{id}}$.

As forementioned, at its full, original resolution, the curvature and torsion plots of discrete knots are not reliable since they contain small scale details which must be seen as artifacts of the discretization. Their origin has been explained in [14]. The amplitude of the artifact details is reduced when, instead of the full set of vertices, we take into consideration m times smaller set obtained by averaging coordinates of m consecutive vertices. The knot obtained in such a manner will be denoted by $K_p^{(m)}$. The higher m, the more efficient the reduction of artifacts. On the other hand, m cannot be too high since this would smear out all subtle details of the knot shape. As a rule we shall be using $m = 10$. At this value of m the number of vertices becomes reduced to $N^{(10)} = 20\,064$ which is still about ten times more than the number of vertices in any of knots analyzed in the past. The averaging positions of $m = 10$ consecutive vertices makes the distance between them approximately ten times longer. Obviously, such a procedure introduces the dispersion of the edge length. However, since the original length of the edges in the K_p knot is extremely small, their dispersion in the $K_p^{(10)}$ knot is negligible. (The relative difference between the longest and shortest knot is of the order 10^{-7}.) Consequently, the Rawdon construction of the inscribed knot can be performed without any problems. A polygonal knot with the reduced number of vertices will be denoted $K_p^{(m)}$. The knot inscribed into it will be denoted by $K_c^{(m)}$.

To grasp the shape of the whole knot one needs to analyze only one sixth of it, i.e. for $l \in [0, L/6)$. In view of the very small difference between the lengths of the K_c and $K_c^{(m)}$

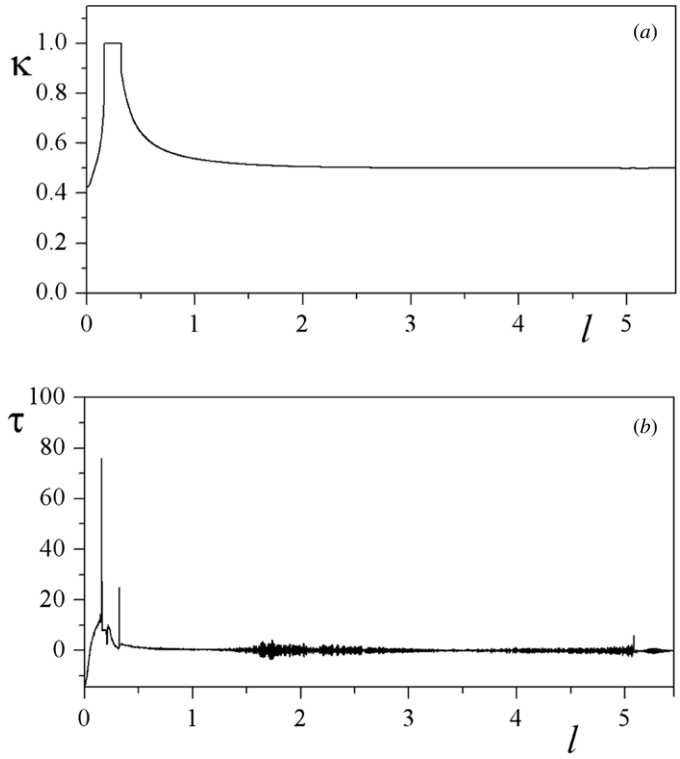

Figure 5. Curvature and torsion of the $K_c^{(10)}$ knot within the $[0, L/6)$ interval.

knots, to describe the plots of curvature and torsion we use the knot length parameter denoted simply as L.

Figure 5 presents the curvature plot of the $K_c^{(10)}$ knot within the representative $1/6$ part of it. As clearly seen in the initial part of the plot the curvature here reaches its upper allowable value $\kappa = 1$. This happens at a well defined, finite interval. The middle and the end parts of the curvature plot seem to be smooth. In what follows we shall demonstrate that this is not true. The maximum curvature interval is separated from the rest of the plot by short pieces with very steep slopes. The steepness of the slopes becomes more visible when we look at a picture of the curvature plot enlarged on the interesting region (see figure 6(*a*)). The shape of the curvature plot presented in the figure convinces us that we are dealing here with what in the ideal trefoil will appear as true discontinuities. In what follows the discontinuities will be referred to as *primary*. We feel allowed to formulate the following.

Conjecture 1 (Present authors)**.** *Curvature of the ideal trefoil knot is not continuous. It reaches the maximum allowable value* $\kappa = 1$ *on six finite intervals. The plateaus of maximum curvature are separated at both sides by discontinuities.*

The values of the arclength parameter at which the primary discontinuities of curvature appear are $l_1 = 0.158 \pm 0.001$ and $l_2 = 0.319 \pm 0.001$, thus the arclength width of the $\kappa = 1$ interval equals $\Delta l_{1,2} = l_2 - l_1 = 0.161 \pm 0.002$, which is more than the 0.122 found by Ashton *et al* from the analysis of their $N = 2400$ knot [12]. The heights of the curvature jumps at both ends of each of the curvature peaks are: $\Delta\kappa_1 = 0.264 \pm 0.005$ and $\Delta\kappa_2 = 0.115 \pm 0.005$.

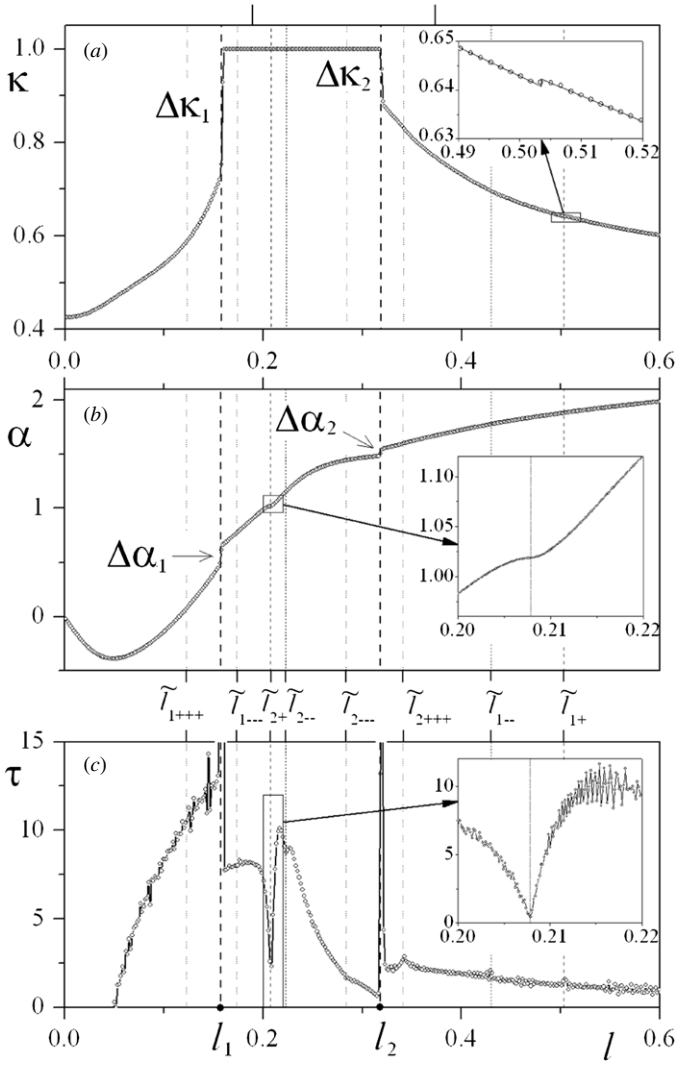

Figure 6. Curvature (*a*), accumulated torsion (*b*) and torsion (*c*) of the $K_c^{(10)}$ knot in the initial part of the $[0, L/6)$ interval. The curvature plot is clearly discontinuous at l_1 and l_2. The torsion plot displays sharp and high peaks (their upper parts are not visible). As we guessed, the peaks turn within the ideal trefoil knot into Dirac deltas. Note that values of torsion at both sides of the peaks are different.

Values of $\Delta\kappa_1$ and $\Delta\kappa_2$ cannot be confronted with results of other works, since the conjecture that curvature of the ideal trefoil knot is discontinuous was not formulated before.

Due to needing the third derivatives of the position vector field, the torsion of the $K_c^{(10)}$ knot is more difficult to determine. Figure 5(*b*) presents the torsion of the $K_c^{(10)}$ knot within the representative $1/6$ part of it. As seen in the figure, the level of noise is much higher than in the curvature plots. Nevertheless, in the interesting region of the curvature peak, where curvature displays discontinuities, one can easily see two very sharp peaks. A study of the behavior of the torsion peaks at varying m reveals that as m decreases, the peaks become sharper and their height increases. Our conclusion is that, what the peaks represent is not a conventional

maxima of a smooth torsion function, but Dirac delta components of the function. Thus, the following hypothesis concerning torsion of the ideal trefoil seems to be well justified:

Conjecture 2 (Present authors)**.** *The torsion of the ideal trefoil is not a conventional function: in points, where the curvature displays primary discontinuities, the torsion displays Dirac delta components.*

The weights of the Dirac delta components of torsion can be estimated by the inspection of the accumulated torsion $\alpha(l)$ plot (see figure 6(*b*)). As seen in the figure, accumulated torsion is discontinuous at l_1 and l_2. The heights of the discontinuities are $\Delta\alpha_1 = 0.159 \pm 0.005$ and $\Delta\alpha_2 = 0.062 \pm 0.005$. The values stay in a quantitative (but not qualitative) conflict with the observation made in [11], since it does not happen in the ideal trefoil knot ...*that the angle ...between adjacent arcs corresponds to an angle of around 70°*. (70° amounts to about 1.2 radians.) The weights of the Dirac delta components of torsion, i.e. the angles between the adjacent arcs, at the places at which as Carlen *et al* conjectured the Frenet frame, become discontinuous, are an order of magnitude smaller than 1.2 radians. A further detailed inspection of the torsion plot, see figure 6(*c*), reveals that values of torsion at both sides of the Dirac delta peaks are different. Thus, our conclusion is that at l_1 and l_2 torsion is also discontinuous.

There is an additional, unexpected feature of the torsion function. As seen in figure 6(*c*), inside the (l_1, l_2) interval it displays a sharp, cusp shaped minimum located at the point marked as $\tilde{l}_{2+}$. As we guessed, the torsion function of the ideal trefoil knot is continuous but not smooth at the point. What is the origin of this singularity? To answer this question we must take into account contact between the points of the K_p knot.

5.3. Contact set and contact functions

Following the notation used by Gerlach [16], let us denote by $\boldsymbol{\gamma}(l)$, $l \in [0, L_{\mathrm{id}})$, the vector function describing the spatial positions of points along the searched for ideal trefoil knot $\mathcal{K}_{\mathrm{id}}$. Here L_{id} is the length of the knot. Each point $\boldsymbol{\gamma}(l)$ of the ideal trefoil knot $\mathcal{K}_{\mathrm{id}}$ can be seen as the center of a single, disc-shaped section $D(l)$ of the perfect rope in which the knot has been tightened. The section discs cannot overlap, but they may be in contact. There are two kinds of contact:

(1) contact between discs from two arclength distant parts of the rope,
(2) contact between neighboring discs.

The first set of contact points will be denoted by $\mathrm{CS_I}$. The second set of contacts will be denoted by $\mathrm{CS_{II}}$. The pieces of the rope, within which contacts of the second type are present, are called kinks [6]. The curvature here reaches its highest possible value $\kappa = 1$. There are two kinds of kinks. In the first kind, present within the simple clasp structure discussed in section 3, section discs stay in contact at a single point. The axis of the rope remains planar here and can be seen as a circular arc of unit radius. In the second kind, the contact points between infinitesimally close discs are not gathered in the same place, but are distributed along a curve in a continuous manner. The simplest object within which such a curve of contacts of the second kind can be found is the perfect rope shaped into a curvature limited helix [17]. See figure 7.

Numerical simulations suggest that each point of the ideal trefoil knot stays in contact of the first kind with exactly two other points of the knot. Simulations described in [12, 15, 16, 18, 19] indicate the contact set $\mathrm{CS_I}$ of the ideal trefoil knot is shaped into a continuous, self-avoiding, knotted curve. The contact set $\mathrm{CS_{II}}$ has not been considered so far. The location of both contact sets within the knot structure is shown in figure 8.

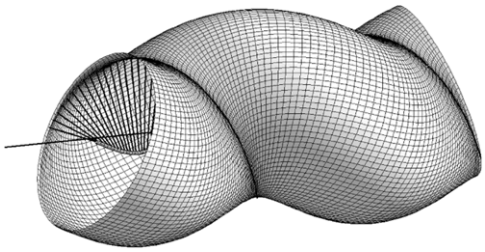

Figure 7. Curvature limited helix [17]. The perfect rope of radius $R = 1$ has been formed into a helix. The radius of the helix $r_H = 0.2$, while its pitch $P_H = 2.513\,27$. At such parameter values the curvature of the helix is equal to 1. Points of contacts of type II draw a helical line on the surface of the rope. The contact points coincide with the centers of the oscillating circles. Some radii that join the centers of the oscillating circles along with the points at which they are tangent to the helix are also shown.

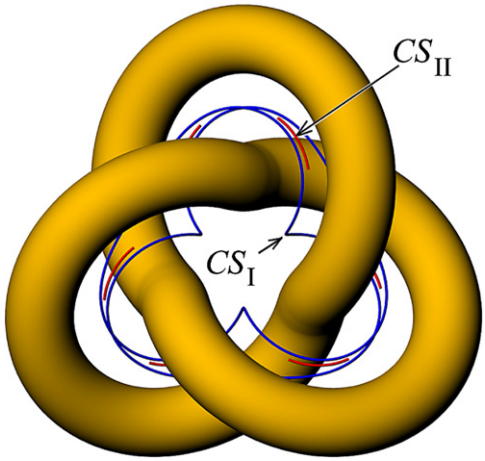

Figure 8. Conjectured location of the contact sets $\mathrm{CS_I}$ and $\mathrm{CS_{II}}$ within the ideal trefoil knot as determined via the analysis of the K_p knot. Contact set $\mathrm{CS_I}$ is connected and knotted. Contact set $\mathrm{CS_{II}}$ consists of six congruent pieces. The arrow indicates one of them.

The points belonging to those parts of the knot, where $\kappa = 1$, should be seen as having not two, but three contacts—the third one being of the second kind. This is essential since, when considering the equilibrium of forces within the ideal trefoil knot (one may imagine that the perfect rope in which it has been tied is subject to tension), the presence of contacts of the second type must be also taken into account. From the physical point of view, the SP-FEM algorithm simulates a knotted, closed rope subject to a longitudinal tension. The tension, acting along the rope, creates at its curved parts the transverse force that pushes vertices from the different parts of the knot toward each other. The SP-FEM algorithm produces additional vertex–vertex forces aimed to prevent the distance between the vertices becoming smaller than 2. On the other hand, the tension present within the simulated rope tries, in some places, to bend it further than it is allowed. In such places, the SP-FEM algorithm produces an additional momenta of forces that are preventing it. As a result, the inscribed knot K_c is free from overlaps and nowhere does its curvature exceed 1. Following notation used by Gerlach [16], we introduce two functions that allow one to indicate those points of the knot that have the

first type of contact. Gerlach denotes the functions as $\sigma(l)$ and $\tau(l)$. Using these functions the pair of the knot points that get in contact, of the first type, with a chosen point $\boldsymbol{\gamma}(l)$ of the knot can be specified as $\boldsymbol{\gamma}(\sigma(l))$ and $\boldsymbol{\gamma}(\tau(l))$. In accordance with a long tradition, τ is used in the present paper as a symbol of torsion, we shall in what follows denote the Gerlach contact functions as σ_- and σ_+. Using the notation, the points at which the contacts of the first kind take place are:

$$\boldsymbol{c}_-(l) = \frac{\boldsymbol{\gamma}(l) + \boldsymbol{\gamma}(\sigma_-(l))}{2}, \tag{8}$$

$$\boldsymbol{c}_+(l) = \frac{\boldsymbol{\gamma}(l) + \boldsymbol{\gamma}(\sigma_+(l))}{2}. \tag{9}$$

Obviously, to determine and parametrize the complete curve of the contact points $\mathrm{CS_I}$ we need only one of the contact function, e.g.:

$$\mathrm{CS_I}(l) = \frac{\boldsymbol{\gamma}(l) + \boldsymbol{\gamma}(\sigma_-(l))}{2}, \ l \in [0, L_{\mathrm{id}}). \tag{10}$$

Let us return to the analysis of the polygonal K_p knot found by the SP-FEM simulation and consider the problem of the contact functions. Approximate discrete images of the functions have been presented in the references [12, 15, 16, 18]. As mentioned above, the SP-FEM algorithm analyzes the vertex–vertex distances (the vertices belonging to different parts of the simulated rope) and whenever they become smaller than 2, it introduces a pair of opposite forces aiming to remove the violations. From the physical point of view, the two vertices between which the forces are acting can be seen as connected with a strut, subject to a compression. When in the course of the SP-FEM simulation the forces acting on a strut change sign, the strut is removed. Thus, at the end of the simulation, the simulation code provides us with the set B of the pairs of vertices between which the compressed, distance keeping struts are present. Vertices connected by a strut can be seen as staying in contact of the first kind. The contact point is located in the middle of the strut. The numerical analysis shows that the absolute deviation of the strut lengths from their desired value 2 is not larger than 8×10^{-15}.

Let $\left\{i_k^B, j_k^B\right\}, k = 1, 2, \ldots, M$, be the pairs of indices defining the struts in the final K_p knot. The ordered pairs $(l_{i_k^B}, l_{j_k^B})$ and $(l_{j_k^B}, l_{i_k^B})$ define, within the $[0, L_p] \times [0, L_p]$, square points that can be seen as pixels of a high but finite resolution, discrete image of the continuous contact functions $\sigma_-(l)$ and $\sigma_+(l)$ (see figure 9). An appropriate processing of the data allows us to find values of the strictly monotone $\sigma_-(l)$ and $\sigma_+(l)$ functions. By analyzing the functions we are able to draw some new conclusions concerning their properties. It is essential to acknowledge that in the view of the conjectured D_3 symmetry of the ideal trefoil knot, to know the shape of both the contact functions in the whole $[0, L_{\mathrm{id}}$ range, it is sufficient to know the shape of one of them in the initial $[0, L_{\mathrm{id}}/3)$ interval or the shapes of both functions in the $[0, L_{\mathrm{id}}/6)$ interval.

To provide proof that the contact curve is knotted, Gerlach formulates a hypothesis (5.14 in [16]), that the contact functions are smooth. The inspection of the plots presented in [12, 15, 16, 18, 19] seems to confirm it. At the first sight, see figure 9, the results of the present study also stay in agreement with the hypothesis. However, inspecting the derivatives of the functions we clearly see this is not the case: see figure 10 and figure 11. The most distinct discontinuities of the derivative of the σ_- function are located at l_1 and l_2 where the curvature displays its primary discontinuities. It is clear that the function is also not smooth at other points. The analysis of the positions and values of the discontinuities and the relations between them requires a separate study.

Another of the hypotheses formulated both by Gerlach and Carlen [16, 19] is the existence within the ideal trefoil of the so-called 9-cycles. A plot of the σ^9 function obtained with the

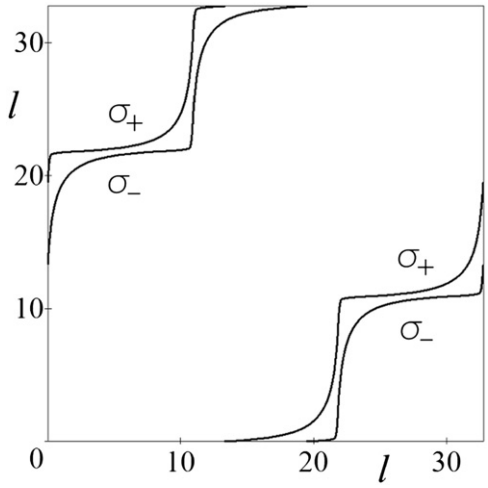

Figure 9. Shapes of the contact functions σ_- and σ_+ as seen via plots of the end points of the contact struts.

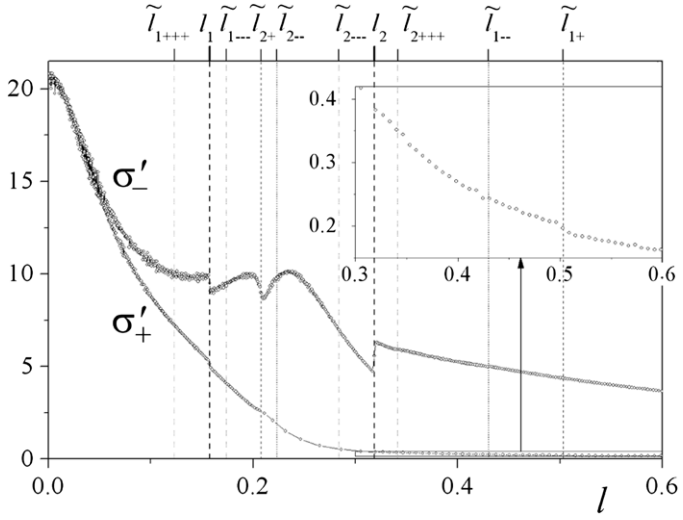

Figure 10. Shape of the derivatives of the contact functions σ_- and σ_+ in the initial part of the $[0, L_c/6)$ interval.

data stemming from the K_p knot indicates that it is not tangent to the diagonal, but intersects it at 18 points. See figure 12. The 18 points form two stable 9-cycles. The arclength positions of the points of the first and second cycle (listed in the order in which they are connected in a given cycle via consecutive actions of the contact function σ_-) are: $C^9_- = [0.189, 15.674, 32.370, 11.103, 26.588, 10.541, 22.018, 4.759, 21.455]$ and $C^9_+ = [\,32.554, 11.288, 27.984, 10.725, 22.202, 6.155, 21.640, 0.373, 17.069]$. We denoted the two cycles by C^9_- and C^9_+ since, although map $l \to \sigma^9_-(l)$ has 18 fixed points, only nine of them gathered in C^9_-, are stable. The other nine fixed points, gathered in C^9_+, prove to be stable from the point of view of mapping $l \to \sigma^9_+(l)$.

The location of the 9-cycles within the spatial structure of the knot is shown in figure 13. As Carlen indicates [19], assuming that symmetry of the ideal trefoil is D_3, the existence of a

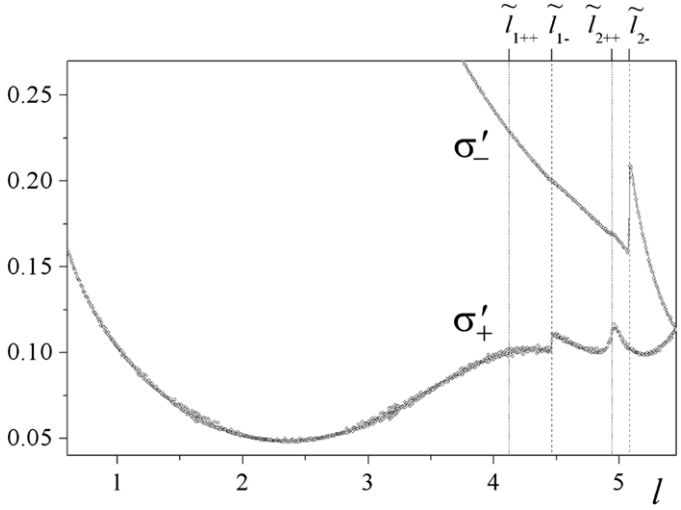

Figure 11. Shape of the derivatives of the contact functions σ_- and σ_+ in the end part of the $[0, L_c/6)$ interval.

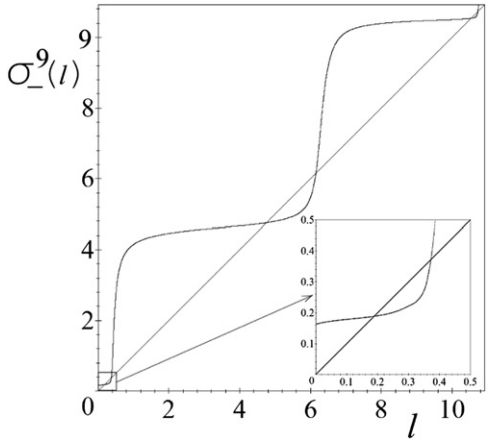

Figure 12. The shape of the 9th functional power σ_-^9 of the contact function σ_- determined from the SP-FEM struts data. To make the intersection points of the σ_-^9 plot with the diagonal we only plotted $1/3$ part of the function. Here there are 6 intersection points, thus, in the whole knot there are 18 of them.

single 9-cycle allows one to construct the whole knot from only two pieces of it. The results of the present study lead to a modification of the statement. Since, as we have demonstrated, we deal not just with one, but with two 9-cycles, the construction of the whole knot needs not two but three pieces[1].

6. Higher order singularities of curvature and torsion

Assuming that the ideal knot has the D_3 symmetry and by properly choosing the place at which the arclength l variable has its origin, we come to the conclusion that what happens in

[1] The old data analyzed in PhD theses by Gerlach and Carlen suggested the existence of a single 9-cycle, but their new data indicate that there are two such cycles.

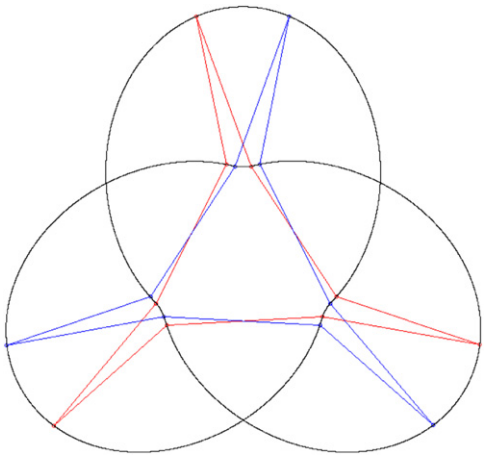

Figure 13. Conjectured position of two 9-cycles within the ideal trefoil knot.

the knot at a point $\boldsymbol{\gamma}(l)$, where $l \in [0, L_{\mathrm{id}}/6)$, happens also at five other points $\boldsymbol{\gamma}(L_{\mathrm{id}}/3 - l)$, $\boldsymbol{\gamma}(L_{\mathrm{id}}/3 + l)$, $\boldsymbol{\gamma}(2L_{\mathrm{id}}/3 - l)$, $\boldsymbol{\gamma}(2L_{\mathrm{id}}/3 + l)$, and $\boldsymbol{\gamma}(L_{\mathrm{id}} - l)$. Obviously, the inverse is also true: whatever happens at $\boldsymbol{\gamma}(l)$, where $l \in [L_{\mathrm{id}}/6, L_i)$, happens also at a $\boldsymbol{\gamma}(\tilde{l})$, where $\tilde{l} \in [0, L_{\mathrm{id}}/6)$. The formulae given above make it clear how to calculate the $\tilde{l}$ value:

$$\tilde{l} = \begin{cases} l & \text{for} \quad l \in [0/L_{\mathrm{id}}/6) & \text{(I)} \\ 2L_{\mathrm{id}}/6 - l & \text{for} \quad l \in [L_{\mathrm{id}}/6, 2L_{\mathrm{id}}/6) & \text{(II)} \\ l - 2L_{\mathrm{id}}/6 & \text{for} \quad l \in [2L_{\mathrm{id}}/6, 3L_{\mathrm{id}}/6) & \text{(III)} \\ 4L_{\mathrm{id}}/6 - l & \text{for} \quad l \in [3L_{\mathrm{id}}/6, 4L_{\mathrm{id}}/6) & \text{(IV)} \\ l - 4L_{\mathrm{id}}/6 & \text{for} \quad l \in [4L_{\mathrm{id}}/6, 5L_{\mathrm{id}}/6) & \text{(V)} \\ L_{\mathrm{id}} - l & \text{for} \quad l \in [5L_{\mathrm{id}}/6, L_{\mathrm{id}}) & \text{(VI).} \end{cases} \tag{11}$$

Suppose we start from point $l_2 = 0.3185$ (located within the $[0, L_{\mathrm{id}}/6)$ interval) at which the primary discontinuity of curvature takes place. The l_2 point stays in contact with point $l_{2-} = \sigma_-(2_1) = 16.7467$. Since $l_{2-} \in [3L_{\mathrm{id}}/6, 4L_{\mathrm{id}}/6)$, $\tilde{l}_{2-} = 4L_{\mathrm{id}}/6 - l_{2-} = 5.0819$. Thus, the influence of the primary discontinuity of curvature located at l_2 on the shape of curvature at the $\sigma_-(2_1)$ should be visible in the representative $[0, L_{\mathrm{id}}/6)$ interval at $\tilde{l}_{2-}$. Inspection of the curvature plot presented in figure 5 is disappointing, since at this value of l the curvature plot seems to be smooth. However, an appropriate magnification reveals interesting details. As seen in the figure 14, the curvature is also discontinuous at the point. This discontinuity will be called *secondary*. Its height equals $0.000\,95 \pm 0.000\,08$. Further inspection of the figure indicates that the accumulated torsion, part (b) of the figure, is also discontinuous. Thus, the torsion shown in part (c) should have a Dirac delta component. Indeed, at $\tilde{l}_{2-}$ the torsion displays at a very high peak. The height of the peak depends strongly on m and thus it represents a Dirac delta component. The weight of the component (equal to the height of the accumulated torsion discontinuity) amounts to 0.0215 ± 0.0016.

Continuing the analysis we may ask what influence the l_2 discontinuity has on the shape of the knot at the point indicated by the second, i.e. σ_+, contact function. The place within the $[0, L/6)$ interval, where it should be seen is located at $\tilde{l}_{2+} = 0.2079$. As seen in figure 6(a) the point falls into the (l_1, l_2) interval, where the curvature is limited by its upper allowable value $\kappa = 1$. Thus, looking at the curvature plot, we do not see anything. Inspection of the accumulated torsion and torsion plots, (b) and (c), reveals that the contact leaves a visible trace: the accumulated torsion has a kind of an inflection point there. Torsion displays at

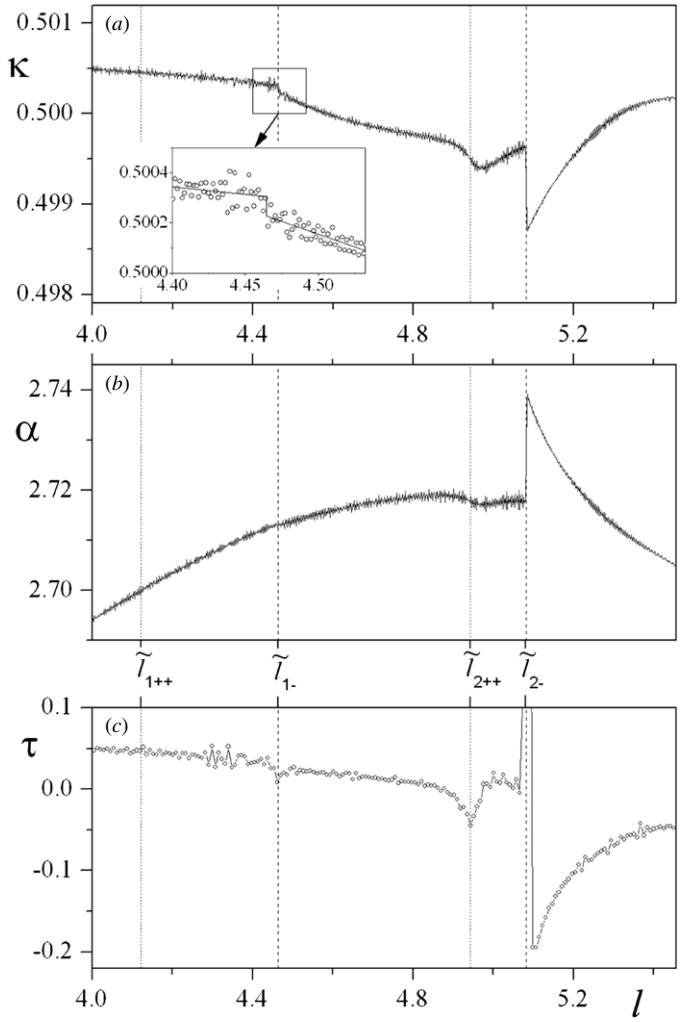

Figure 14. Enlarged plots of curvature (a), accumulated torsion (b) and torsion(c), in the end part of the $[0, L/6)$ interval. The secondary discontinuity of curvature visible at $\tilde{l}_{2-}$ is induced by the primary discontinuity visible in figure 6(a) at l_2.

the point a sharp, cusp shaped minimum. Our conjecture is that at the $\tilde{l}_{2+}$ point of the ideal trefoil knot its torsion is continuous but not smooth. There it reaches its zero value.

Similar analysis allows one to indicate the origin of the other interesting landmarks visible in the curvature and torsion plots. For instance, the secondary discontinuity of curvature shown in the picture inserted in figure 6(a) is located at $\tilde{l}_{1+} = 0.5029$ point. Its height amounts to 0.0016 ± 0.0008, thus it is very small. The secondary discontinuity shown in the picture inserted in figure 14(a) is located at $\tilde{l}_{1-} = 4.463\,61$ and its height is hardly visible: $0.000\,05 \pm 0.000\,05$. Ternary singularities located at points $\tilde{l}_{1--}$ and $\tilde{l}_{1++}$ are much weaker. It seems that at $\tilde{l}_{2--}$ and $\tilde{l}_{2++}$ there are no singularities, since $\tilde{l}_{2+}$ is located within the interval of constant curvature and the same happens with $\tilde{l}_{2--}$. We managed to detect some of them, but since their magnitudes are burdened with large errors, we do not list them.

7. Conclusions

The results of the simulations presented above allowed us to formulate firmly supported conjectures concerning the shape of the ideal conformation of the closed trefoil knot. Let us gather them into a single list.

(1) Curvature κ of the ideal trefoil is not continuous. The primary discontinuities appear at the ends of the intervals within which $\kappa = 1$.
(2) Torsion τ of the ideal trefoil knot is not continuous. Localization of its singularities is identical with localization of the discontinuities of curvature. At the points of the primary discontinuities of curvature, the torsion function has singular Dirac delta components.
(3) Contact functions of the ideal trefoil knot are not smooth. The points of their discontinuities are related to the discontinuities of curvature and torsion.
(4) The ideal trefoil knot hosts two 9-cycles.
(5) Contacts between various parts of the ideal trefoil knot propagate each of its primary shape singularities along the knot, but the existence of the constant curvature intervals and the 9-cycles makes the propagation process decay.

These new conjectures, listed above, essentially change our view on the shape of the ideal trefoil knot, indicating that it is more complex than it has been assumed so far. Let us emphasize that acceptance of the existence in the ideal knot of shape singularities was possible only because we kept in mind results of the Starostin and Sullivan study of the simple clasp. In a similar manner, the existence of the secondary shape singularities and their connections with the primary singularities became clear only due to the idea of the contact functions introduced by Carlen and Gerlach. The curvature, torsion and contact functions singularities are closely related. A general study of the connections between them still needs some more work.

Acknowledgments

John Sullivan and Evgueni Starostin drew our attention to the simple clasp problem and to its analytical solution. They patiently explained to us the importance of the subtle details of its structure. Jason Cantarella drew our attention to the problem of local minima. Eric Rawdon taught us how to properly analyze the polygonal knots produced by SONO and SP-FEM. PhD theses of Henryk Gerlach and Mathias Carlen helped us to understand the importance of the contact functions and indicated possibility of the existence of 9-cycles. Rob Kusner gave us the moral support necessary to complete the work. We thank all of them. The work was supported by Poznan University of Technology grant 06/62/DSPB/0214/2014.

References

[1] Cantarella J, Kusner R B and Sullivan J M 2002 On the minimum ropelength of knots and links *Invent. Math.* **150** 257–86
[2] Cantarella J, LaPointe A and Rawdon E J 2012 Shapes of tight composite knots *J. Phys. A: Math. Theor.* **45** 225202
[3] Sullivan J M 2003 The tight clasp *Electron. Geom. Models* **2001.11.001** (www.eg-models.de/models/Curves/Space_Curves/2001.11.001/_direct_link.html)
[4] Starostin E L 2003 A constructive approach to modelling the tight shapes of some linked structures *Forma* **18** 263–93 (www.scipress.org/journals/forma/pdf/1804/18040263.pdf)
[5] Cantarella J, Fu J H G, Kusner R B, Sullivan J M and Wrinkle N C 2006 Criticality for the Gehring link problem *Geom. Topology* **10** 2055–115
[6] Cantarella J, Fu J H G, Kusner R B and Sullivan J M 2013 Ropelength criticality *Geom. Topology* at press (arXiv:1102.3234)

[7] Przybyl S and Pieranski P 2009 Tightening of the elastic overhand knot *Phys. Rev.* E **79** 031801
[8] Katritch V, Bednar J, Michoud D, Scharein R G, Dubochet J and Stasiak A 1996 Geometry and physics of knots *Nature* **384** 142–5
[9] Pieranski P 1996 Poszukiwanie wezlow idealnych *ProDialog* **5** 111–20
[10] Rawdon E J 2003 Can computers discover ideal knots? *Exp. Math.* **12** 287–302
[11] Carlen M, Laurie B, Maddocks J H and Smutny J 2005 Biarcs, global radius of curvature and the computation of ideal knots *Physical and Numerical Models in Knot Theory (Series on Knots and Everything* vol 36*)* ed J A Calvo, K C Millett, E J Rawdon and A Stasiak (Singapore: World Scientific) chapter 5
[12] Ashton T, Cantarella J, Piatek M and Rawdon E J 2011 Knot tightening by constrained gradient descent *Exp. Math.* **20** 57–90
[13] Baranska J, Przybyl S, Pieranski P and Rawdon E J 2004 Length of the tightest trefoil knot *Phys. Rev.* E **70** 051810
[14] Baranska J, Przybyl S and Pieranski P 2008 Curvature and torsion of the tight closed trefoil knot *Eur. Phys. J.* B **66** 547–56
[15] Pieranski P and Przybyl S 2001 Ideal trefoil knot *Phys. Rev.* E **64** 031801
[16] Gerlach H 2010 Ideal knots and other packing problems of tubes *PhD Thesis* EPFL, Lausanne
[17] Przybyl S and Pieranski P 2001 Helical close packings of ideal ropes *Eur. Phys. J.* E **4** 445–9
[18] Smutny J 2004 Global radii of curvature, and the biarc approximation of space curves: in pursuit of ideal knot shapes *PhD Thesis* EPFL, Lausanne
[19] Carlen M 2010 Computation and visualization of ideal knot shapes *PhD Thesis* EPFL, Lausanne